PROCEEDINGS REPRINT

SPIE—The International Society for Optical Engineering

Reprinted from

Neutron Optical Devices and Applications

22–24 July 1992
San Diego, California

Volume 1738

Invited Paper

Subsurface profile refinement for neutron specular reflectivity

John F. Ankner and Charles F. Majkrzak

National Institute of Standards and Technology
Reactor Radiation Division, Gaithersburg, MD 20899

ABSTRACT

The importance of modeling in the analysis of neutron and x-ray reflectivity data cannot be overstated. For specular reflectivity, the theory is straightforward and one merely needs a flexible platform for constructing density profiles. We will describe the parameters used in and the limitations of such models.

1. INTRODUCTION

The use of neutron and x-ray reflectivity to obtain the structure of surfaces, thin films and multilayers has become widespread during the past several years.[1–3] A cursory analysis of the intensity measured as a function of specular reflection angle can reveal general information about sample quality, as well as obvious layer thicknesses within the sample (e.g. the bilayer spacing in an artificial metal superlattice). One can, however, by careful modeling extract much more information from a reflectivity measurement than just bilayer spacing.

Calculating the specular reflectivity of neutrons or x-rays from an arbitrary number of refracting slabs is a straightforward problem solved many years ago.[4,5] If it were possible to measure both the amplitude and phase of the reflected beam, data analysis would simply consist of a direct transform of this information back to a refractive index profile. However, as is the case with conventional diffraction, one can only measure intensity (amplitude squared). For any given scan of intensity versus angle, there exists an infinity of possible refractive index profiles—which defines the so-called uniqueness problem. Of course, not all of these profiles are physically reasonable and one can reduce the volume of parameter space to be searched by applying "reasonability" constraints. Therefore, the fundamental requirement of specular reflectivity modeling is to amass as much information about the sample as possible before sitting down to fit the data. This information typically consists of nominal individual layer thicknesses and refractive indices and the order in which they were deposited, as well as the estimated length scale of the mixing between these layers.

Even under optimal conditions, there exist fundamental limitations on the quality of the structural information available in specular reflectivity. Since the momentum transfer in the scattering process is normal to the sample surface, one cannot measure any in-plane correlations. The most

 0-8194-0911-1/92/$4.00

important consequence of this is the well-known inability to distinguish between a surface that is truly rough and one that is interdiffused. In other words, one cannot determine the length scale of the in-plane structures responsible for smearing out features in the specular reflectivity. As this is often crucial for the determination of the physical properties of a film or multilayer, one would like to have some way of obtaining this information. By measuring scattering at momentum transfers off of the specular and thereby introducing a wavevector component in the plane of the film, one can in principle determine these correlations although, as for specular reflectivity, not uniquely. A number of groups are currently at work on the theoretical treatment of off-specular scattering—hopefully, in the near future the methods discussed here will be adapted for use in modelling in-plane structures.[15–17]

By employing a mixture of flexible software, knowledge of the sample from other techniques, and a healthy dose of skepticism, one can obtain meaningful structural information from a fit of the specularly reflected intensity. In the next section, we will outline the theory of reflectivity from a stratified medium, followed in section 3 by a hopefully illustrative discussion of a simple case, and in section 4 by something a bit more challenging. Along the way, we will sprinkle the path with the expected cautions for the unwary and admonitions to the unwise.

2. THEORY OF SPECULAR REFLECTIVITY

Neutrons and x rays, in their quantum-mechanical wave-like properties, obey the laws of classical optics. For most materials, the refractive index is slightly less than one [deviating by $O(10^{-5}\text{-}10^{-6})$],

$$n_l = \sqrt{1 - \lambda^2 N_l b_l/\pi}, \tag{1}$$

where λ is the wavelength of the radiation, N_l the number density of the scatterers, and b_l their scattering length. The scattering length is a complex number, with the imaginary part related to the mass absorption coefficients of the constituent atoms. The specular reflectivity from a surface or interface is described by the one-dimensional wave equation. Fig. 1 shows the relevant wavevectors for specular scattering for an L-layer system. For specular reflectivity, the angle of incidence equals the angle of exit, $\phi_i = \phi_f \equiv \phi$. The solution of this problem for $L = 1$ is trivial and its extension to multiple layers follows simply by keeping proper account of the boundary conditions for layers inserted between the incident medium and substrate. This process can be expressed as a recursion relation,[5]

$$R_{l-1} = a_{l-1}^4 \left[\frac{R_l + F_{l-1,l}}{R_l F_{l-1,l} + 1}\right], \tag{2}$$

where

$$R_l = a_l^2 \left(\frac{r_l}{t_l}\right), \tag{3}$$

$$a_l = \exp(ik_{zl}d_l/2), \tag{4}$$

and

$$F_{l-1,l} = \frac{k_{zl-1} - k_{zl}}{k_{zl-1} + k_{zl}}. \tag{5}$$

The recursion variable R_l consists of the ratio between reflection and transmission coefficients in

layer l multiplied by a phase factor a_l^2, which depends on the layer thickness d_l. In this formula, the reflection coefficient in the incident medium r_0 is determined by starting at the substrate ($R_L = r_L = 0$) and stepping through the reflecting layers until emerging into the incident medium ($r_0 = R_0$, assuming t_0 is normalized to unit intensity). The Fresnel factor $F_{l-1,l}$ contains the angular dependence of the reflectivity and embodies Snell's Law through the refraction-corrected wavevectors

$$k_{zl} = \sqrt{k_z^2 - 4\pi N_l b_l}, \tag{6}$$

where $k_z = 2\pi \sin\phi/\lambda$ is the component of the incident wavevector in vacuum normal to the surface. By means of this recursion relation, one can calculate the exact specular reflectivity from an arbitrary number of layers.

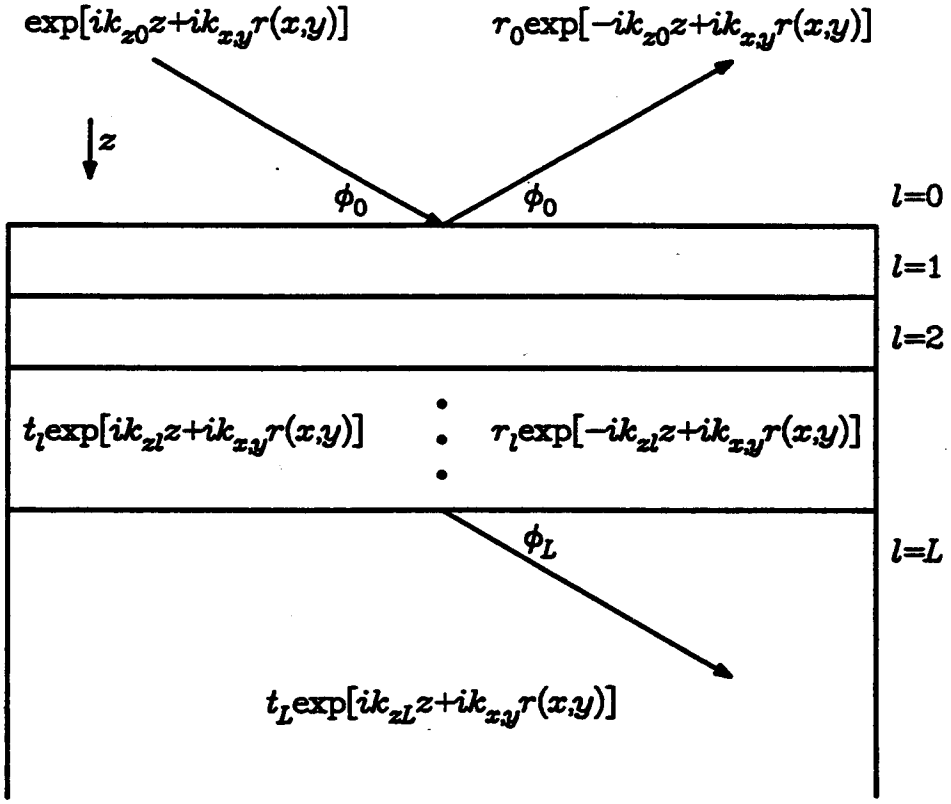

Figure 1: Geometry and wavefields for specular reflectivity from a stratified medium. A plane wave $\exp ik_{z0}z + ik_{x,y}r(x,y)$ strikes a flat interface at incident angle ϕ_0 from a medium of refractive index n_0, exciting specularly reflected and refracted beams. The amplitudes and phases of these beams are contained in the coefficients r_l and t_l and may be calculated by satisfying the boundary conditions on the neutron wavefunction Ψ: at an refractive index step Ψ and $\vec{\nabla}\Psi \cdot \hat{z}$ are continuous. The boundary conditions imply that the in-plane x and y components of the wavevectors do not change.

3. REFLECTIVITY FROM A SINGLE OVERLAYER

Now that we have dispensed with general principles, how does one apply these principles to the fitting of actual data—in particular, how does one construct a refractive-index profile? The solid dots in Fig. 2 are reflected intensity data, normalized to unit incident intensity, measured as a function of normal wavevector $Q = 2k_z = 4\pi \sin\phi/\lambda$, taken from a sample consisting of a single nickel layer of nominal 1000 Å thickness sputtered[6] onto a float glass substrate. Now, the scattering density of bulk Ni and glass are well known and may be used as input parameters for an initial guess. As can be seen from Fig. 2a, the calculated reflectivity differs markedly from the measured. In order to reconcile our model curve with the data, we must first account for instrumental resolution. The BT-7 reflectometer at the National Institute of Standards and Technology reactor, on which this data was taken, is a double axis diffractometer with the beam wavelength selected from a Maxwellian spectrum by means of Bragg diffraction from a graphite monochromator and with the incident beam defined by slits.[7] The Q resolution of such an instrument may be described as follows:

$$\delta Q = Q\sqrt{(\delta\phi \cot\phi)^2 + \left(\frac{\delta\lambda}{\lambda}\right)^2}, \tag{7}$$

where $\delta\phi$ is the angular divergence of the incident beam (0.3 mradian in this case), λ the nominal wavelength of the neutrons (2.37 Å), and $\delta\lambda$ the wavelength spread (0.02 Å). Fig. 2b shows our initial guess convoluted with a Gaussian of full width δQ at each data point (note that δQ is not constant, but increases monotonically with Q, so the convolution must be carried out point-by-point).

Several fairly substantial problems remain in our quest to match naive expectation to harsh reality: the critical reflection angle of the model is too large, the rapid oscillations are not in phase with those of the data, and the envelope does not intersect the data at large Q. The first two of the above can be resolved by adjusting the scattering density and thickness of the Ni layer. The solid line in Fig. 2c results from first reducing the Ni scattering density so that the model goes through the data near Q_c and then increasing the nickel thickness until the first several oscillations line up. Finally, we must lower the model envelope function. Interfacial mixing, a combination of roughness and interdiffusion, lowers the reflectivity at each interface and thereby reduces the intensity of features on the model curve. Up to now, we have assumed that the interfaces in the film are perfectly sharp, so that the profile can be represented in terms of step functions,

$$\rho(z) = \rho_{\mathrm{Ni}}\Theta(z - z_0) + (\rho_{\mathrm{glass}} - \rho_{\mathrm{Ni}})\Theta(z - z_0 - d_{\mathrm{Ni}}), \tag{8}$$

where $\rho = Nb$ is the scattering-length density, $z_0 > 0$ is an arbitrary depth where the vacuum/Ni interface is placed, d_{Ni} is the thickness of the nickel layer, and Θ is the Heaviside unit step function[8] ($\Theta(z) = 0$ for $z < 0$ and 1 for $z \geq 0$). In the real world, roughness and interdiffusion act to smear these perfect interfaces, such that

$$\begin{aligned}\rho(z) = \rho_{\mathrm{Ni}} \int_0^z dz' I(z - z', \sigma_{\mathrm{vacuum/Ni}})\Theta(z' - z_0) \\ +(\rho_{\mathrm{glass}} - \rho_{\mathrm{Ni}}) \int_0^z dz' I(z - z', \sigma_{\mathrm{Ni/glass}})\Theta(z' - z_0 - d_{\mathrm{Ni}}).\end{aligned} \tag{9}$$

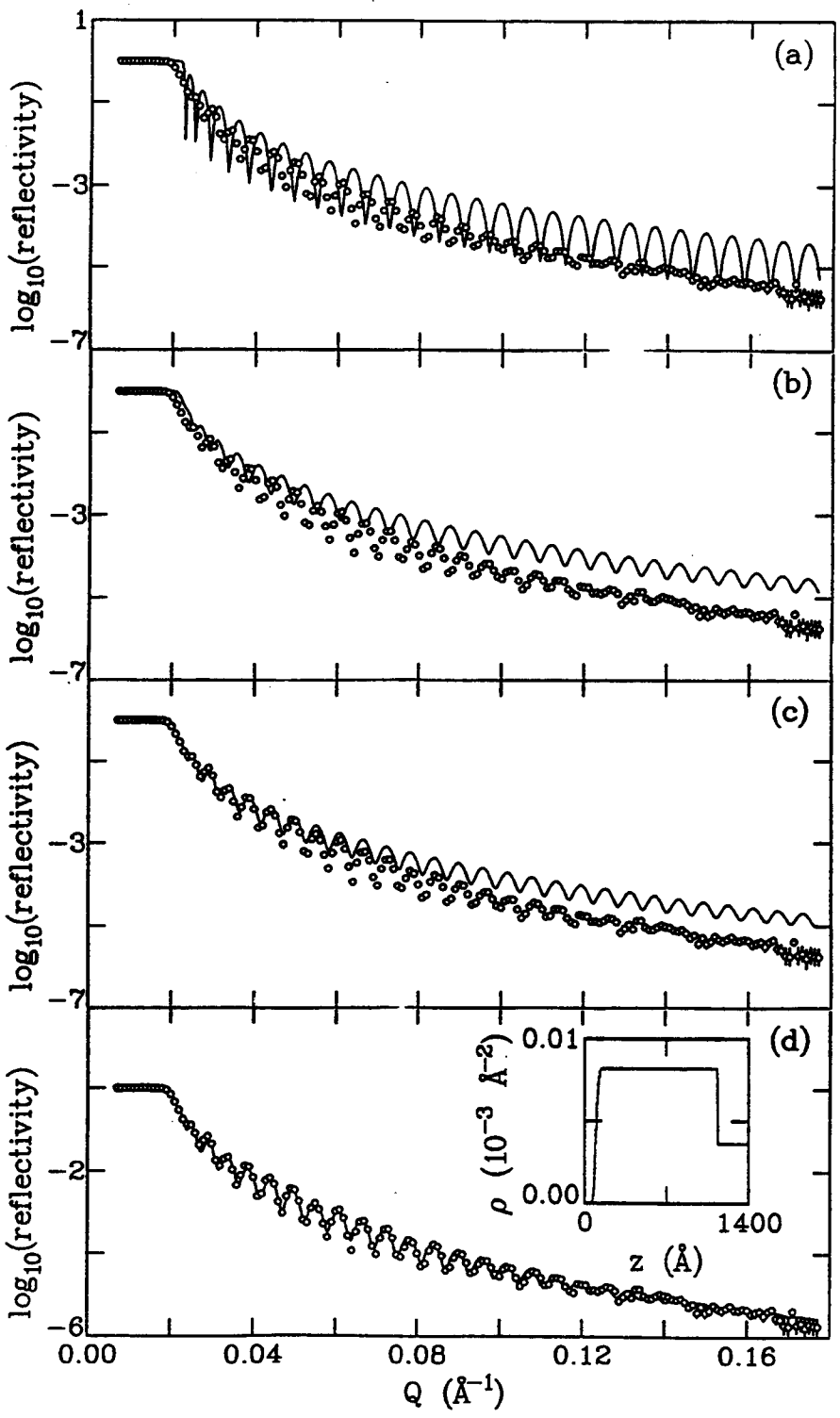

Figure 2: Sequence of steps in the fitting of a single Ni layer. (a) An initial guess based on prior knowledge of the film. (b) Our initial guess corrected for instrumental resolution. (c) Adjustment of the scattering density and thickness of the film so that the low-Q features line up. (d) Final fit including variation of interfacial mixing—inset shows fitted density profile.

Table 1: Parameters from fit to Ni film specular reflectivity data.

l	Type	ρ (Å^{-2})	d (Å)	σ (Å)
1	Ni	$8.2 \cdot 10^{-6}$	1042	15.6
2	glass	$3.6 \cdot 10^{-6}$	—	2.7

The functions $I(z,\sigma)$ are convoluted with the scattering density steps and round off their sharp edges. The most commonly used interfacial function is the Gaussian

$$I(z,\sigma) = \frac{1}{\sigma\sqrt{2\pi}} e^{-z^2/2\sigma^2}, \tag{10}$$

where σ is its characteristic width (approximately equal to the half-width at half maximum). The convolution of a Gaussian with a unit step Θ yields an error function. By discretizing the error function as a series of small density increments, we can generate a complete scattering density profile based on equation (9), calculate its specular reflectivity using (2), and vary the interfacial width parameters σ, layer thickness d, and scattering density ρ using a non-linear least squares fit routine[9] to minimize χ^2. Our best fit to the data is shown in Fig. 2d with the profile inset and the parameters listed in Table 1.

Now that all of the dust has settled, what information have we extracted from our fit? First, the fitted scattering density for Ni is only 0.87 that of the bulk, meaning that a substantial amount of space in the film is occupied by voids and grain boundaries. In addition, we have determined the thickness of the film to within ±2 Å by means of the constraint placed on this parameter by the large number of oscillations present in the data. Finally, we find a small interfacial mixing at the Ni/glass interface and a rather larger roughness at the vacuum/Ni. One would expect some oxide formation at the surface, but since the bulk scattering density of NiO differs from that of Ni by less than 3%, this oxide is essentially invisible although it probably accounts for much of the observed roughening.

4. MULTILAYER REFLECTIVITY

The preceding example represents just about the simplest possible application of specular reflectivity analysis. However, the principles used in that analysis can be applied to systems of arbitrary complexity, limited only by available computing power and the patience of the experimenter.

Table 2: Parameters from fit to NiC/TiMn multilayer specular reflectivity data.

l	Type	ρ (Å^{-2})	d (Å)	σ (Å)
1	NiO	$9.6 \cdot 10^{-6}$	51.3	15.7
2, 4, ..., 18	TiMn	$0.9 \cdot 10^{-6}$	56.8	9.4
3, 5, ..., 19	NiC	$9.9 \cdot 10^{-6}$	36.2	9.4
20	TiMn	$-0.8 \cdot 10^{-6}$	53.7	9.4
21	glass	$3.6 \cdot 10^{-6}$	—	2.1

The generalization of equation (9) is straightforward, with

$$\rho(z) = \rho_0 + \sum_{l=1}^{L}(\rho_l - \rho_{l-1}) \int_0^z dz' I(z - z', \sigma_l)\Theta(z' - z_l), \tag{11}$$

where $z_l - z_0$ is the depth of interface l below the surface,

$$z_l = z_0 + \sum_{l'=1}^{l} d_{l'} \tag{12}$$

and the summation runs over the L layers in the film (see Fig. 1). Note that the incident medium ($l = 0$) need not be vacuum. Indeed, since the absorption of thermal neutrons by such materials as silicon, quartz (SiO_2) and sapphire (Al_2O_3) is small, a great deal of neutron work on solid/liquid interfaces has been done using thick blocks of these materials as the incident medium.[10]

The additional complexity present in multiple-layer reflecting systems poses a number of problems for modeling. All of these problems are essentially related to the fact that a much larger amount of information must be extracted from a data set of approximately the same size as that of a single-layer system (compare the number of data points in Figs. 2 and 3—in each case about 200). One must decide which information is most important and construct a model such that a minimum number of additional parameters is required.

The sample whose reflectivity is plotted in Fig. 3 is a multilayer consisting of ten alternating layers of sputtered NiC and TiMn—a potential neutron supermirror material. Two important requirements for the optimal performance of supermirror layers are that the interfaces between layers be sharp and that the scattering density contrast be as large as possible. Co-deposition of Ni and C (both materials with large positive scattering lengths and number densities) alternately with TiMn (a negative scattering length alloy) represents one possible means of improving supermirror performance. The film discussed here was grown[6] to study the feasibility of this approach. A brief glance at the inset to Fig. 3a (the fitted profile to which the solid line corresponds) reveals two related problems: first, the interfaces are quite rounded and, second, the contrast between the layers is substantially less than expected. In fact, we see from Table 2 that not only does the NiC layer exhibit only about two-thirds of its expected density ($\sim 14 \cdot 10^{-6}$ Å^{-2}), but the TiMn density is not even negative (expected to be $\sim -2 \cdot 10^{-6}$ Å^{-2}). The large alteration in scattering density but comparatively small interfacial roughness indicates that interdiffusion has occurred to such an extent that the composition of the NiC and TiMn layers has been altered in a more-or-less homogeneous fashion. These results are discussed in greater detail elsewhere in this volume.[11]

The model we have chosen is not perfect, as can be seen from Fig. 3a, but is sufficient for us to be able to extract the information discussed above. How sensitive is the fit to the parameters in Table 2 and what effect do these parameters have on the model curve? The superlattice periodicity is our main interest, so naturally we are most concerned that the fit does well at the three measured superlattice peaks. However, these peaks ride on an envelope produced by the non-periodic elements of the structure, namely the subsidiary maxima (Kiessig fringes) caused by the total film thickness and the long-Q "swell" associated with the broken-symmetry layers at the vacuum and substrate. All of these periodicities interfere coherently, so one cannot simply ignore the non-symmetric layers and just fit the superlattice peaks. So, we have fitted an oxide layer at the top and a separate

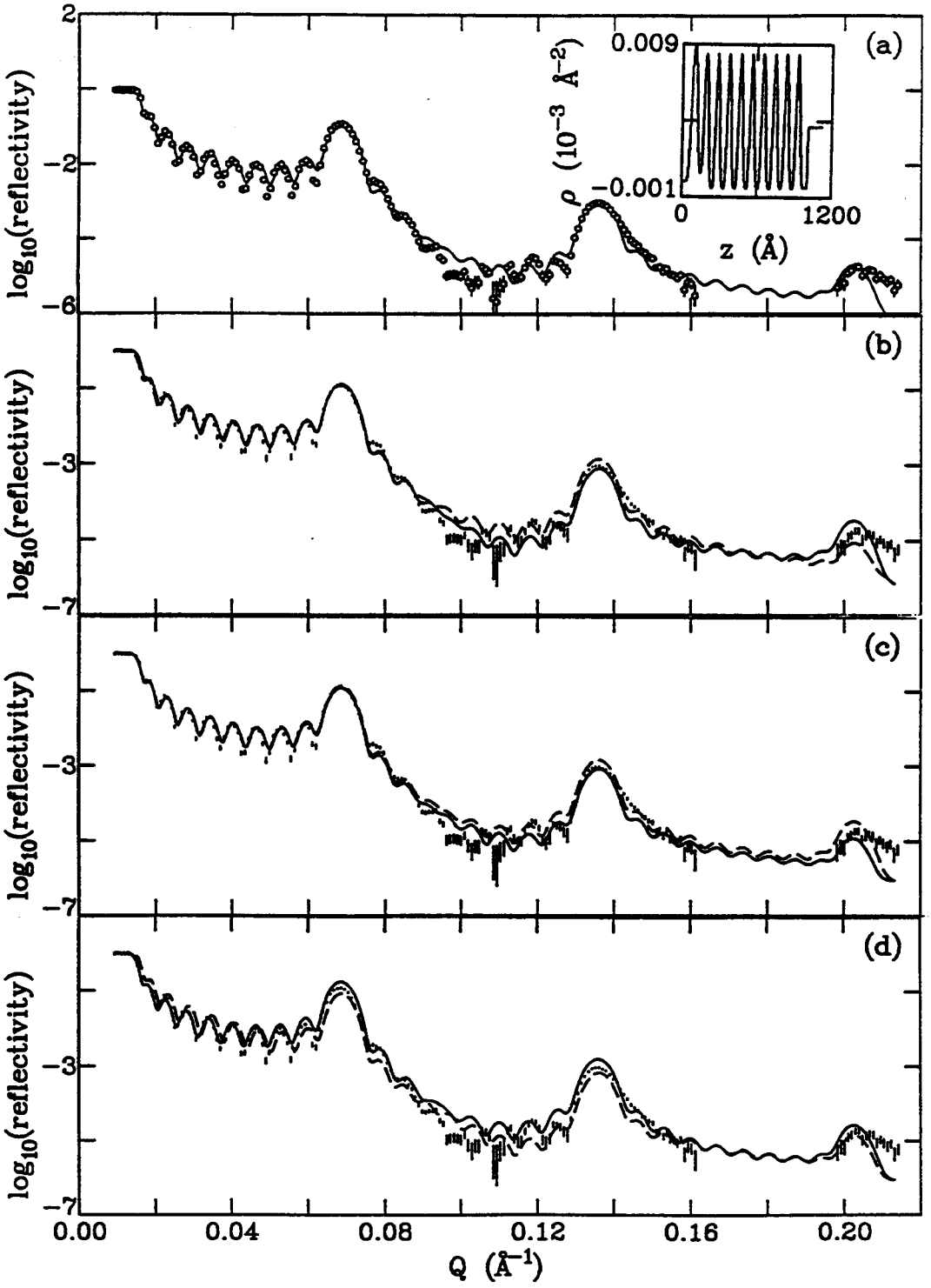

Figure 3: Models of multilayer reflectivity. (a) Best-fit to the NiC/TiMn multilayer described in the text; inset shows a plot of the real part of the scattering density versus depth. (b) Variation of layer thicknesses about best-fit values: dashed—d_{NiC}+2 Å, $d_{\mathrm{TiMn}} - 2$ Å; solid—reverse. (c) Variation of multilayer interfacial mixing: $\sigma \pm 2$ Å, for solid and dashed, respectively. (d) Variation of scattering densities ρ: solid corresponds to $\rho_{\mathrm{NiC}} + 1. \cdot 10^{-6}$ Å^{-2} and $\rho_{\mathrm{TiMn}} - 1. \cdot 10^{-6}$ Å^{-2}; dashed corresponds to the reverse.

TiMn layer immediately adjacent to the substrate. The parameters obtained agree rather well with the single-layer results in Table 1, particularly the mixing (σ) at the vacuum/NiO and TiMn/glass interfaces. Another interesting result is that layer 20, the TiMn in contact with the glass, more closely approaches the expected scattering density, indicating that interdiffusion is less prevalent when only one layer interface contacts the NiC. We were able to get the long-Q envelope basically correct simply by altering layers 1 and 20; the remainder of the film, layers 2–19, is periodic.

The effects of the various multilayer fit parameters on the model curve shape are shown in Fig. 2b–d. Figure 2b shows the data plotted as error bars, with the dashed line corresponding to d_{TiMn} offset from the values in Table 2 by +2 Å and d_{NiC} by –2 Å and the solid line to the reverse situation; 2c shows σ offset ±2 Å for solid and dashed lines, respectively; and in 2d the solid line represents ρ_{NiC} and ρ_{TiMn} values $2 \cdot 10^{-6}$ Å^{-2} farther apart, with dashed being the same amount closer together. We can infer some general rules about the behavior of the fit parameters from these plots. Variation of the d spacings causes a redistribution of intensity among the superlattice peaks, while the mixing σ increasingly dampens the intensity of the higher-order peaks, and density ρ changes all the heights by about the same amount. It is important to note that the only parameter that has any effect on the first-order peak is is the density contrast. This rule applies generally: except in the case of enormous roughness, the first-order superlattice peak is unaffected by σ and the individual ds, although it gives a good estimate of overall bilayer spacing. By observing the intensity variation of the superlattice peaks (the more the better), one can obtain an estimate of the density profile.

In choosing the model for this data, we proceeded from simple to more complex and stopped when the fit seemed good enough for us to be able to trust the numbers it produced. Occam's Razor must be applied rigorously and without pity. If a fitted parameter cannot be correlated with any measurable change in the model reflectivity or if a model with fewer layers or greater symmetry fits just as well, the parameter is not seen in the data and the simpler model prevails.

5. CONCLUSION AND NEW DIRECTIONS

We have outlined the theory of specular reflectivity modeling and presented an algorithm for the implementation of a layer-by-layer non-linear least squares fit routine. In terms of the two examples discussed here, our explicit layer-generating approach is equivalent to the static Debye-Waller method[12] employed by other workers. Our technique is more general, however, because it can be applied to interfaces that cannot be described as rounded rectangular blocks, such as parabolic polymer segment density profiles[10] and magnetic films with dead layers.[13] One merely has to replace the step function Θ in equation (11) with the appropriate ideal profile to be convoluted with $I(z, \sigma)$.

Currently, we are developing a program to fit simultaneously the four cross sections that can be measured with a fully polarized neutron reflectometer[7] and thereby to carry out the quantitative analysis of spin-flip magnetic reflectivity experiments. Eventually, it should be possible to model off-specular reflectivity by similar methods to those described here—for instance, by employing the transmission amplitudes t_l from equation (2) in the distorted-wave Born approximation.[14]

At our current level of understanding, one cannot, in general, determine a unique solution from reflected intensity data. This fact is both distressing and encouraging. Distressing because one can never be sure of an answer or know when to quit; encouraging because there still remain problems to tax the ingenuity of the ambitious or foolhardy.

6. REFERENCES

1. C.F. Majkrzak and G.P. Felcher, Mater. Res. Soc. Bull. 15 (11), 65–72 (1990).
2. J. Penfold and R.K. Thomas, J. Phys. C 2, 1369 (1990).
3. T.P. Russell, Mat. Sci. Rep. 5, 171 (1990).
4. F. Abelés, Ann. Phys. Fr. 12, 596 (1950).
5. L.G. Parratt, Phys. Rev. 95, 359 (1954).
6. Both of the films described in this work were made by the Opto-Line Corporation, Andover, MA, 01810.
7. C.F. Majkrzak, Physica B 173, 75 (1991).
8. W. Kaplan, *Advanced Mathematics for Engineers*, Addison-Wesley, Reading, MA, 1981, ch. 4.
9. W.H. Press, B.P. Flannery, S.A. Teukolsky, and W.T. Vetterling, *Numerical Recipes*, Cambridge University Press, Cambridge, 1986, ch. 14.
10. S.K. Satija, in this volume.
11. C.F. Majkrzak and J.F. Ankner, in this volume.
12. L. Nevot and P. Croce, Rev. Phys. Appl. 15, 761 (1980).
13. C.F. Majkrzak, N.F. Berk, J.F. Ankner, and S.K. Satija, in this volume.
14. J.F. Ankner, in *Surface X-Ray and Neutron Scattering*, edited by H. Zabel and I.K. Robinson, Springer Proceedings in Physics, Vol. 61, Springer-Verlag, New York, 1992, p. 105.
15. S.K. Sinha, E.B. Sirota, S. Garoff, and H.B. Stanley, Phys. Rev. B 38, 2297 (1988).
16. S.K. Sinha, M.K. Sanyal, A. Gibaud, S.K. Satija, C.F. Majkrzak, and H. Homma, in NATO Advanced Study Institute Conference Proceedings (Greece, June 26, 1990).
17. R. Pynn, Phys. Rev. B 45, 602 (1992).